2840 *Chem. Mater.* **2009,** *21,* 2840–2845
DOI:10.1021/cm900511g

CHEMISTRY OF MATERIALS
Article

Cruciforms: Assembling Single Crystal Micro- and Nanostructures from One to Three Dimensions and Their Applications in Organic Field-Effect Transistors

Chengliang Wang,[†,§] Yaling Liu,[†,§] Zhuoyu Ji,[†,§] Erjing Wang,[†,§] Rongjin Li,[†,§] Hui Jiang,[†] Qingxin Tang,[†] Hongxiang Li,*[,‡] and Wenping Hu*[,†]

[†]*Beijing National Laboratory for Molecular Sciences, Key Laboratory of Organic Solids, Institute of Chemistry, Chinese Academy of Sciences, Beijing 100190, China,* [‡]*Laboratory of Material Science, Shanghai Institute of Organic Chemistry, Chinese Academy of Sciences, Shanghai, 200032 China, and* [§]*Graduate University of Chinese Academy of Sciences, Beijing 100039, China*

Received February 19, 2009. Revised Manuscript Received April 26, 2009

The self-assembly behaviors and charge transport properties of cruciforms with anthracene as one axis were studied. By changing one axis of these cruciforms, the assembly morphologies of single crystal micro/nanostructures transferred from one dimension to three dimensions. This morphology transformation was controlled by the intermolecular interactions of cruciforms, which was proved by single crystal X-ray diffraction results and presented a facile way to synthesize different dimensional micro/nanostructures through molecular design. Field-effect transistors based on individual single crystal micro/nanostructure exhibited high performance. These results suggested the potential applications of cruciform in organic electronics.

Introduction

The morphological difference of micro- and nanosized organic semiconductors, such as one-dimensional to three-dimensional (1D to 3D) micro/nanostructures, usually brings bulky changes to properties and plays an important role in organic electronics.[1−20] Recently, 1D micro- and nanostructures have attracted much attention, and great progress has been made.[7−17] However, due to the uncontrollability of intermolecular interactions ($\pi-\pi$ interaction, $C-H\cdots\pi$ interaction, hydrogen bond, van der Waals interaction, etc.) and complexities of self-assembly process, morphology control of organic micro/nanostructures is still a great challenge and lags behind that of inorganic materials at the current stage.[18−20] What is more, to tune the assembly morphology of organic semiconductors by molecular design is rarely reported, although it is very helpful to understand the mystery of self-assembly and is one of the superiorities of organic materials compared with inorganic ones. Herein, using cruciforms as candidates, we achieved the tuning of organic micro/nanostructures from 1D to 3D by careful molecular design.

Cruciforms are a family of materials that have two distinct molecular axes with either similar or dissimilar branches. They have received significant attention because of their unique shapes and properties and have been used in sensors, nonlinear optical materials, and organic

*Corresponding authors. E-mail: lhx@mail.sioc.ac.cn; huwp@iccas.ac.cn.

(1) Hu, J.; Odom, T. W.; Lieber, C. M. *Acc. Chem. Res.* **1999**, *32*, 435.
(2) Whitesides, G. M.; Grzybowski, B. *Science* **2002**, *295*, 2418.
(3) Kim, D. H.; Lee, D. Y.; Lee, H. S.; Lee, W. H.; Kim, Y. H.; Han, J. I.; Cho, K. *Adv. Mater.* **2007**, *19*, 678.
(4) Yip, H.; Ma, H.; Jen, A. K.-Y.; Dong, J.; Parviz, B. A. *J. Am. Chem. Soc.* **2006**, *128*, 5672.
(5) Hu, J.; Guo, Y.; Liang, H.; Wan, L.; Jiang, L. *J. Am. Chem. Soc.* **2005**, *127*, 17090.
(6) Aleshin, A. N. *Adv. Mater.* **2006**, *18*, 17.
(7) Tang, Q.; Jiang, L.; Tong, Y.; Li, H.; Liu, Y.; Wang, Z.; Hu, W.; Liu, Y.; Zhu, D. *Adv. Mater.* **2008**, *20*, 2947.
(8) Briseno, A. L.; Mannsfeld, S. C. B.; Jenekhe, S. A.; Bao, Z.; Xia, Y. *Mater. Today* **2008**, *11*, 38.
(9) Lee, S. J.; Hupp, J. T.; Nguyen, S. T. *J. Am. Chem. Soc.* **2008**, *130*, 9632.
(10) O'Carroll, D.; Iacopino, D.; O'Riordan, A.; Lovera, P.; O'Conor, É.; O'Brien, G. A.; Redmond, G. *Adv. Mater.* **2008**, *20*, 42.
(11) Zhou, Y.; Liu, W.; Ma, Y.; Wang, H.; Qi, L.; Cao, Y.; Wang, J.; Pei, J. *J. Am. Chem. Soc.* **2007**, *129*, 12386.
(12) Briseno, A. L.; Mannsfeld, S. C. B.; Lu, X.; Xiong, Y.; Jenekhe, S. A.; Bao, Z.; Xia, Y. *Nano Lett.* **2007**, *7*, 668.
(13) Briseno, A. L.; Mannsfeld, S. C. B.; Reese, C.; Hancock, J. M.; Xiong, Y.; Jenekhe, S. A.; Bao, Z.; Xia, Y. *Nano Lett.* **2007**, *7*, 2847.
(14) Zhao, Y.; Fu, H.; Hu, F.; Peng, A.; Yang, W.; Yao, J. *Adv. Mater.* **2008**, *20*, 79.
(15) Nguyen, T.; Martel, R.; Avouris, P.; Bushey, M. L.; Brus, L.; Nuckolls, C. *J. Am. Chem. Soc.* **2004**, *126*, 5234.
(16) Balakrishnan, K.; Datar, A.; Zhang, W.; Yang, X.; Naddo, T.; Huang, J.; Zuo, J.; Yen, M.; Moore, J. S.; Zang, L. *J. Am. Chem. Soc.* **2006**, *128*, 6576.
(17) Tang, Q.; Li, H.; He, M.; Hu, W.; Liu, C.; Chen, K.; Wang, C.; Liu, Y.; Zhu, D. *Adv. Mater.* **2006**, *18*, 65.
(18) Benedetto, F. D.; Camposeo, A.; Pagliara, S.; Mele, E.; Persano, L.; Stabile, R.; Cingolani, R.; Pisignano, D. *Nat. Nanotechnol.* **2008**, *3*, 614.
(19) Zhang, X.; Zhang, X.; Zou, K.; Lee, C.-S.; Lee, S.-T. *J. Am. Chem. Soc.* **2007**, *129*, 3527.
(20) Jiang, L.; Fu, Y.; Li, H.; Hu, W. *J. Am. Chem. Soc.* **2008**, *130*, 3937.

 Published on Web 05/14/2009

Scheme 1. Chemical Structures of Compounds BPEA 1a, BNEA 1b, and BTEA 1c

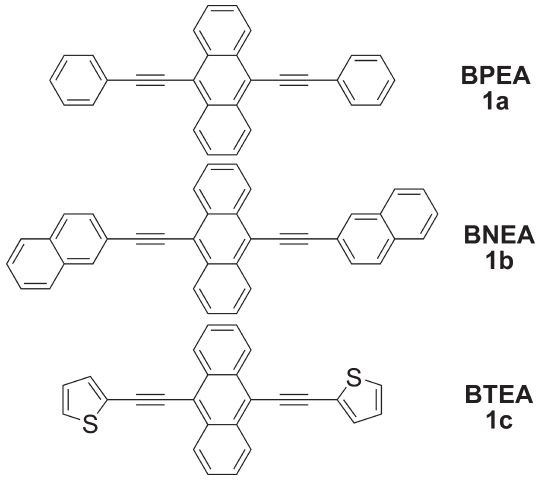

single layer device components,[21−26] though their self-assembly characteristics and applications in nanoelectronics are rarely presented.[27−29] The chemical structures of the cruciforms used in our experiment were shown in Scheme 1. In these cruciforms, anthracene was one axis, and the other axis was formed through substitution on the 9,10-positions of anthracene (simulations have shown that substitutions at the peri position of acenes could lead to π stacking in crystals, which would facilitate charge transport[30−36]). Carbon−carbon triple bonds were introduced to these cruciforms to erase the steric repulsion between two axes.[37] Experimental results showed (i) these cruciforms were easy to form single crystal micro/nanostructures via a simple solution drop-cast process; (ii) 1D to 3D micro/nanostructures were obtained, which was tuned by changing one axis of the cruciforms and presented a facile way to synthesize micro/nanostructures with different dimensions; (iii) slipped $\pi-\pi$ stacking was observed in their single crystals; and (iv) OFETs based on individual micro/nanostructure of cruciforms exhibited high performance (mobility up to 0.73 $cm^2/(V\ s)$ for BPEA **1a**, 0.52 $cm^2/(V\ s)$ for BNEA **1b**, and on/off ratio up to 10^4-10^5 for both **1a** and **1b**).

Experimental Section

General Details. All chemicals and reagents were purchased from commercial suppliers and used without further purification unless otherwise noted. Cruciform **1a** was synthesized according to the literature.[38] UV−vis spectra were recorded on a Hitachi U-3010 spectrometer. Cyclic voltammograms were obtained on a CHI660C analyzer in a conventional three-electrode cell using a glassy carbon working electrode, a platinum wire counter electrode, and an Ag/AgCl reference electrode. X-ray diffraction (XRD) measurements were carried out in the reflection mode using a Rigaku raix Rapid IP area detector X-ray diffraction system (Mo Kα radiation, λ = 0.71073 Å). SEM images were performed on a Hitachi S-4300 SE instrument. TEM images and SAED patterns were carried out on a JEOL JEM-2011 instrument.

9,10-Bis(naphthalen-2-ylethynyl)anthracene (BNEA 1b). A 100 mL flask was charged with 9,10-dibromoanthracene (1.68 g, 5 mmol), copper iodide (115 mg, 0.6 mmol), $Pd(P(Ph)_3)_2Cl_2$ (210 mg, 0.3 mmol), aqueous 2-aminoethanol (2 M, 20 mL), and THF (30 mL) under N_2. After the reaction mixture was degassed three times, 2-naphthylacetylene (1.52 g, 10 mmol) was added. The reaction solution was stirred overnight at 80 °C under N_2 atmosphere. The aqueous layer was extracted with dichloromethane. The combined organic layer was evaporated under reduced pressure. The crude mixture was purified by recrystallization from toluene to provide BNEA **1b** as crystals (yield: 1.6 g, 67%). Mp: 263 °C. MS (EI) *m*/*z*: 478 [M^+]. ^1H NMR (400 MHz, $CDCl_3$): 8.79 (q, 4H), 8.31 (s, 2H), 7.82−7.95 (m, 8H), 7.70 (q, 4H), 7.56 (t, 4H). Anal. Calcd for $C_{38}H_{22}$: C, 95.37; H, 4.63. Found: C, 95.15; H, 4.64.

9,10-Bis(thiophen-2-ylethynyl)anthracene (BTEA 1c). BTEA **1c** was prepared according to a procedure similar to that of **1b**. Yield: 61%. Mp: 276 °C. MS (EI) *m*/*z*: 390 [M^+]. ^1H NMR (400 MHz, $CDCl_3$): 8.62 (q, 4H), 7.65 (q, 4H), 7.51 (d, 2H), 7.42 (d, 2H), 7.13 (t, 2H). Anal. Calcd for $C_{26}H_{14}S_2$: C, 79.96; H, 3.61. Found: C, 79.69; H, 3.67.

Device Fabrication and Electrical Characterization. The SiO_2/Si substrates used were heavily doped *n*-type Si wafer with 500 nm-thick SiO_2 layer and capacitance of 7.5 nF cm^{-2}. After being rinsed with concentrated H_2SO_4/H_2O_2, water, and *iso*-propanol, they were modified with *n*-octodecyltrichlorosilane (OTS). Before solution was drop cast, the substrates were rinsed with hexane, chloroform and *iso*-propanol successively. Single crystals of **1a**−**c** were grown directly onto the OTS-modified SiO_2/Si substrates from chlorobenzene solutions (1 mg/mL). FET devices were fabricated in situ by gluing Au films onto single crystals as drain and source electrodes. Device characteristics were obtained with a Keithley 4200 SCS and Micromanipulator 6150 probe station in a clean and shielded box at room temperature in air.

(21) Miao, Q.; Chi, X.; Xiao, S.; Zeis, R.; Lefenfeld, M.; Siegrist, T.; Steigerwald, M. L.; Nuckolls, C. *J. Am. Chem. Soc.* **2006**, *128*, 1340.
(22) Li, Y.; Wu, Y.; Liu, P.; Prostran, Z.; Gardner, S.; Ong, B. S. *Chem. Mater.* **2007**, *19*, 418.
(23) Schmidt, R.; Göttling, S.; Leusser, D.; Stalke, D.; Krause, A.-M.; Würthner, F. *J. Mater. Chem.* **2006**, *16*, 3708.
(24) Roncali, J.; Leriche, P.; Cravino, A. *Adv. Mater.* **2007**, *19*, 2045.
(25) Zen, A.; Bilge, A.; Galbrecht, F.; Alle, R.; Meerholz, K.; Grenzer, J.; Neher, D.; Scherf, U.; Farrell, T. *J. Am. Chem. Soc.* **2006**, *128*, 3914.
(26) Ponomarenko, S. A.; Tatarinova, E. A.; Muzafarov, A. M.; Kirchmeyer, S.; Brassat, L.; Mourran, A.; Moeller, M.; Setayesh, S.; de Leeuw, D. *Chem. Mater.* **2006**, *18*, 4101.
(27) Hauck, M.; Schönhaber, J.; Zucchero, A. J.; Hardcastle, K. I.; Müller, T. J. J.; Bunz, U. H. F. *J. Org. Chem.* **2007**, *72*, 6714.
(28) Florio, G. M.; Klare, J. E.; Pasamba, M. O.; Werblowsky, T. L.; Hyers, M.; Berne, B. J.; Hybertsen, M. S.; Nuckolls, C.; Flynn, G. W. *Langmuir* **2006**, *22*, 10003.
(29) Zhao, Y.; Xu, J.; Peng, A.; Fu, H.; Ma, Y.; Jiang, L.; Yao, J. *Angew. Chem., Int. Ed.* **2008**, *47*, 7301.
(30) Jurchescu, O. D.; Subramanian, S.; Kline, R. J.; Hudson, S. D.; Anthony, J. E.; Jackson, T. N.; Gundlach, D. J. *Chem. Mater.* **2008**, *20*, 6733.
(31) Jiang, J.; Kaafarani, B. R.; Neckers, D. C. *J. Org. Chem.* **2006**, *71*, 2155.
(32) Subramanian, S.; Park, S. K.; Parkin, S. R.; Podzorov, V.; Jackson, T. N.; Anthony, J. E. *J. Am. Chem. Soc.* **2008**, *130*, 2706.
(33) Tang, M. L.; Reichardt, A. D.; Miyaki, N.; Stolten, R. M.; Bao, Z. *J. Am. Chem. Soc.* **2008**, *130*, 6064.
(34) Curtis, M. D.; Cao, J.; Kampf, J. W. *J. Am. Chem. Soc.* **2004**, *126*, 4318.
(35) Moon, H.; Zeis, R.; Borkent, E.-J.; Besnard, C.; Lovinger, A. J.; Siegrist, T.; Kloc, C.; Bao, Z. *J. Am. Chem. Soc.* **2004**, *126*, 15322.
(36) Anthony, J. E. Chem. Rev. 2006, 106, 5028 and references therein.
(37) Meng, Q.; Gao, J.; Li, R.; Jiang, L.; Wang, C.; Zhao, H.; Liu, C.; Li, L.; Hu, W. *J. Mater. Chem.* **2009**, *19*, 1477.
(38) Swager, T. M.; Gil, C. J.; Wrighton, M. S. *J. Phys. Chem.* **1995**, *99*, 4886.

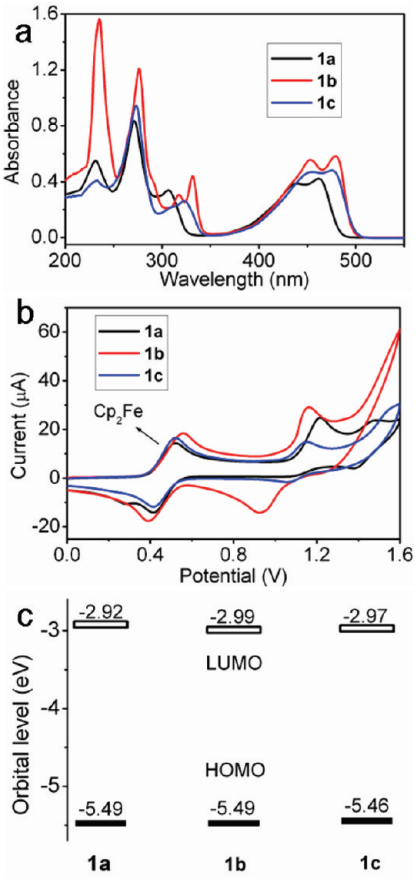

Figure 1. (a) UV−vis absorption spectra, (b) cyclic voltammograms, and (c) orbital levels of BPEA **1a**, BNEA **1b**, and BTEA **1c**.

Results and Discussion

The cruciforms were synthesized through modified Sonogashira reaction in which stronger base aqueous ethanolamine was used to replace trialkylamine.[39] All cruciforms were soluble in normal solvents and could be purified through recrystallization. They were totally characterized by ^{1}H NMR, MS, and elementary analyses.

The absorption spectra of **1a**−**c** in dilute solution were illustrated in Figure 1. According to the UV−vis spectra (Figure 1a), the optical band gaps determined from the initial absorption were 2.57, 2.50, and 2.49 eV for **1a**−**c**, respectively. Cyclic voltammograms of **1a**−**c** showed irreversible oxidation peaks in CH_2Cl_2 solution (Figure 1b). The highest occupied molecular orbital (HOMO) energy levels of these compounds determined at the onset oxidation potentials (using ferrocene as internal standard substance) were −5.49, −5.49, and −5.46 eV for **1a**−**c**, respectively. The similar chemical structures, band gaps, and HOMO/LUMO energy levels (Figure 1c) of these cruciforms made it reasonable to summarize the relationships among chemical structures, molecular arrangements, morphologies, and properties.

With the concentration of BPEA **1a** increasing, a new peak at 310 nm (with a shoulder) was observed (see Supporting Information). At the same time, the initial absorption was red-shifted, and the absorptions peaks became broader. Similar phenomena were observed for BNEA **1b** and BTEA **1c**. The absorption−concentration dependence suggested the strong intermolecular interactions and good self-assembly characteristics of these cruciforms. Figure 2a−c illustrated the scanning electron microscopy (SEM) images of **1a**−**c** self-assembled from chlorobenzene (4 mg/mL) at the same experimental condition using drop-cast method. BPEA **1a** showed 1D micro/nanometer wires with a diameter from hundreds nanometers to several micrometers and length about hundreds micrometers (Figure 2a), BNEA **1b** formed 2D microribbons with a width about tens micrometers and length from tens to hundreds micrometers (Figure 2b), and BTEA **1c** displayed 3D polyhedron morphology (Figure 2c). It is well-known that the assembly morphologies of materials are controlled by their intermolecular interactions. Such 1D to 3D morphology transformation of these materials indicated the marked changes of intermolecular interactions in **1a**−**c**, which could be proved by their single crystal diffraction results.

Single crystals of **1a**−**c** qualified for X-ray diffraction were grown by slow solvent evaporation. The single crystals of **1a**−**c** revealed all compounds had nearly planar structures (The angle between the plane of anthracene and that of the substituents was 0.26° for BPEA **1a**, 10.35° for BNEA **1b**, and 5.72° for BTEA **1c**, respectively).[40] And they adopted herringbone packing in the crystals, similar to that of anthracene[41,42] (see Supporting Information). But different from anthracene at the same time, $\pi-\pi$ stacking was observed in these compounds. This confirmed that the side substitutions facilitated $\pi-\pi$ stacking. Figure 3 showed the packing diagrams of **1a**−**c** along the $\pi-\pi$ stacking direction. For BPEA **1a**, the herringbone angle was 80.5° and the $\pi-\pi$ stacking distance was about 3.46 Å. The $\pi-\pi$ overlap between one BPEA molecule and its adjacent molecules was almost a benzene ring (about 30% of the anthracene plane). Besides the $\pi-\pi$ interactions, there were also C−H$\cdots\pi$ interactions between BPEA and its four neighbor molecules. As for BNEA **1b**, the herringbone angle was 69.6° and the $\pi-\pi$ stacking distance was about 3.44 Å. But there was only about half a benzene ring's $\pi-\pi$ overlap between one BNEA molecule and its adjacent molecules (about 15% of the anthracene plane). Different with BPEA, one BNEA molecule interacted with 10 neighbor molecules through C−H$\cdots\pi$ interactions. This might be resulted from the extending π system, which gave more opportunities to form C−H$\cdots\pi$ interactions. For BTEA **1c**, its packing was very different from those of BPEA and

(39) Ahmed, M. S. M.; Mori, A. *Tetrahedron* **2004**, *60*, 9977.

(40) X-ray data for BPEA **1a**: monoclinic space group $C2/c$, D_c = 1.230 g cm^{-3}, Z = 4, a = 22.866(5) Å, b = 5.3567(11) Å, c = 16.930(3) Å, β = 99.72(3)°, V = 2043.8(7) Å^3. X-ray data for BNEA **1b**: monoclinic space group $P2_1/c$, D_c = 1.244 g cm^{-3}, Z = 2, a = 11.787(2) Å, b = 5.9569(12) Å, c = 18.334(4) Å, β = 97.17(3)°, V = 1277.2(4) Å^3. X-ray data for BTEA **1c**: orthorhombic space group $Pbca$, D_c = 1.404 g cm^3, Z = 8, a = 16.508(3) Å, b = 10.367(2) Å, c = 21.587(4) Å, V = 3694.2(13) Å^3. Details provided as Supporting Information.

(41) Karl, N.; Marktanner, J. *Mol. Cryst. Liq. Cryst.* **2001**, *355*, 149.

(42) Dimitrakopoulos, C. D.; Malenfant, P. R. L. *Adv. Mater.* **2002**, *14*, 99.

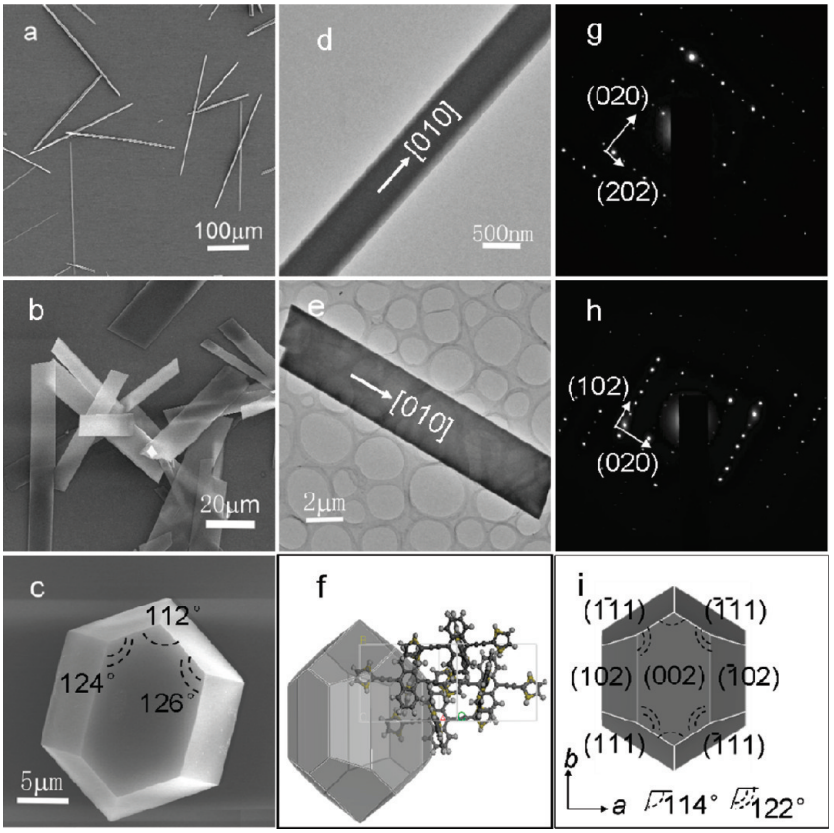

Figure 2. (a, b) SEM images, (d, e) TEM images, and (g, h) SAED patterns of an individual wire or ribbon of **1a**,**b**. (a, d, g) BPEA **1a**; (b, e, h) BNEA **1b**. (c) SEM image and (f, i) theoretically predicted growth morphologies of BTEA **1c** single crystal.

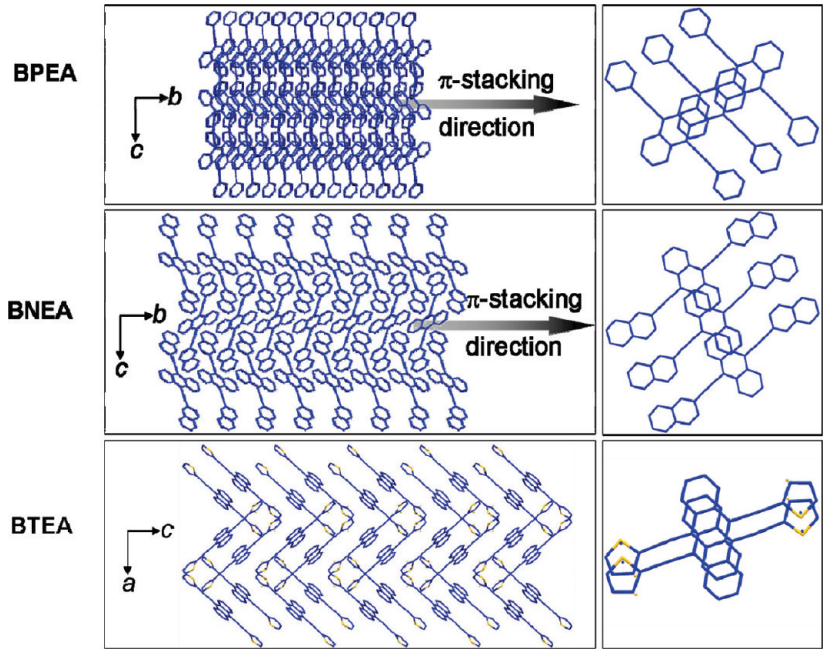

Figure 3. Left: Packing diagrams of BPEA **1a**, BNEA **1b**, and BTEA **1c**. Right: Overlap between adjacent molecules (viewed perpendicularly to the plane of anthracene). Protons are omitted for clarity.

BNEA. Two adjacent molecules of BTEA formed a dimer due to the strong $\pi-\pi$ and S···S interactions (the $\pi-\pi$ overlap and the distance between BTEA molecules in a dimer were two and a half benzene rings (about 83% of the anthracene plane) and 3.51 Å, respectively). Although BTEA exhibited much larger $\pi-\pi$ overlap than those of BPEA and BNEA, there was no $\pi-\pi$ stacking between any two dimers. We attributed this different arrangement to the disorder of the S atom positions and the more complex intermolecular interactions (every BTEA molecule interacted with 12 molecules through short contacts ($\pi-\pi$, C−H···π, and S···S interactions)). From the crystal structures of BTEA, BNEA, and BPEA, the molecular arrangements suggested a tendency that a

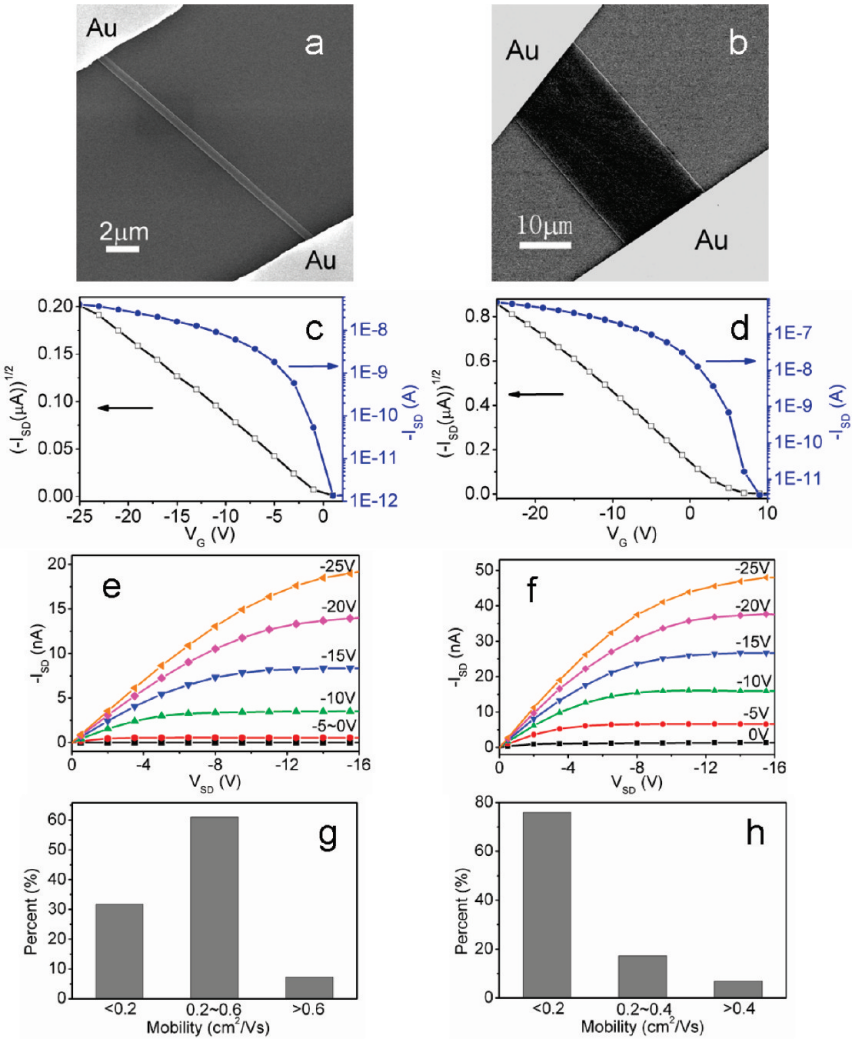

Figure 4. (a, b) the SEM images of an example device based on an individual single crystal of **1a**,**b**; (c, d) their corresponding transfer curve in the saturate regime at a constant source-drain voltage of 30 V and square root of the absolute value of the current as a function of the gate voltage; (e, f) output curves at different gage voltages; and (g, h) mobilities distribution. (a, c, e, g) BPEA **1a**; (b, d, f, h) BNEA **1b**.

long-range $\pi-\pi$ interaction emerged and became dominating gradually in the crystals, and this tendency might be the reason that the assembly morphologies of BTEA, BNEA, and BPEA transformed from 3D to 1D according to the preferred orientation crystal growth mechanism. Transmission electron microscopy (TEM) images and their corresponding selected area electron diffraction (SAED) patterns of an individual micro/nanostructure of BPEA and BNEA are showed in Figure 2d,e,g,h, respectively. No change was observed in the different parts of an individual wire or ribbon, indicating that the whole wire or ribbon was a single crystal. Both compounds grew along the [010] ($\pi-\pi$ stacking) direction, which fit very well with the theoretical calculated results (using the Bravais−Friedel−Donnay−Harker (BFDH) method).[43,44] As a result of the thickness of BTEA, its TEM and SAED patterns could not be obtained. The theoretical predicted BFDH morphology of BTEA is presented (Figure 2f,i). We could see it was nicely consistent with the SEM image (Figure 2c) on the visible shape (Figure 2f) and relative angles (Figure 2i). This consistency suggested that the micro/nanosized crystals of BTEA adopted the same molecular arrangements with the single crystal structure. The SAED data together with BFDH results further proved that the assembly morphologies of **1a**−**c** were determined by their molecular interactions, and the self-assembly mechanism was preferred orientation crystal growth mechanism

The charge transport properties of **1a**−**c** were examined to study their potential applications in OFETs. First, single crystal micro/nanometer wires or ribbons were grown directly on *n*-octadecyltrichlorosilane (OTS) treated SiO_2/Si substrates via drop casting from chlorobenzene solutions. Then transistors were fabricated in situ by gluing Au films onto these micro/nanometer wires or ribbons as source-drain electrodes.[45,46] And the channel was formed simultaneously, along with the lengths about several tens of micrometers and the width depending on

(43) Donnay, J. D. H.; Harker, D. *Am. Mineral.* **1937**, *22*, 446.
(44) Beyer, T.; Day, G. M.; Price, S. L. *J. Am. Chem. Soc.* **2001**, *123*, 5086.
(45) Tang, Q.; Tong, Y.; Li, H.; Hu, W. *Appl. Phys. Lett.* **2008**, *92*, 083309.
(46) Tang, Q.; Tong, Y.; Ji, Z.; Li, H.; Hu, W.; Liu, Y.; Zhu, D. *Adv. Mater.* **2008**, *20*, 1511.

the wires or ribbons themselves. Figure 4 showed the SEM images of an individual micro/nanometer wire and ribbon transistors and their corresponding device characteristics of BPEA and BNEA. More than 30 devices were tested for both BPEA **1a** and BNEA **1b**, and all devices exhibited *p*-type FET properties under ambient conditions. The mobilities were in the range of 0.03 to 0.73 $cm^2/(V\ s)$ for **1a** and 0.01 to 0.52 $cm^2/(V\ s)$ for **1b**, respectively. Statistical results showed more than 70% devices of BPEA exhibited mobilities higher than 0.2 $cm^2/(V\ s)$, while the data for BNEA was only about 20% (Figure 4g−h). The mobilities based on selected thin crystals of BTEA **1c** (10^{-5} $cm^2/(V\ s)$) were much lower than those of **1a**,**b** because of its thickness and disrupted π stacking which hindered charge transport. The device performance (mobility decreased in the sequence of BPEA, BNEA, and BTEA) together with crystal growth of BPEA and BNEA along $\pi-\pi$ stacking direction indicated the strong effect of $\pi-\pi$ interactions to the morphology and mobility.

Conclusion

In summary, nearly planar cruciform organic semiconductors were synthesized, and their self-assembly properties were studied. Morphology tune of single crystal micro/nanostructures from 1D to 3D was facilely achieved by changing one axis of these cruciforms. From BTEA and BNEA to BPEA, the molecular arrangements suggested that a long-range $\pi-\pi$ interaction tended to emerge and become dominating gradually in the crystals, and this tendency was the reason that led to a 3D to 1D assembly morphology transformation. Single crystal field-effect transistors based on individual micro/nanometer-sized wire/ribbon were fabricated and exhibited high performance. All these results suggested the significant roles of intermolecular interactions in morphology control and the potential applications of cruciforms in organic electronics.

Acknowledgment. This work was supported by National Natural Science Foundation of China (60771031, 60736004, 20721061, 50725311), Ministry of Science and Technology of China (2006CB806200, 2006CB932100), and Chinese Academy of Sciences.

Supporting Information Available: UV−vis spectra, fluorescence spectra, and SEM images (PDF) and CIF files of cruciform BPEA, BNEA, and BTEA. This material is available free of charge via the Internet at http://pubs.acs.org.